THE JOURNAL OF PHYSICAL CHEMISTRY A

pubs.acs.org/JPCA Article

Experimental and Theoretical Photoemission Study of Indole and Its Derivatives in the Gas Phase

Oksana Plekan,* Hanan Sa'adeh, Alessandra Ciavardini, Carlo Callegari, Giuseppe Cautero, Carlo Dri, Michele Di Fraia, Kevin C. Prince, Robert Richter, Rudi Sergo, Luigi Stebel, Michele Devetta, Davide Faccialà, Caterina Vozzi, Lorenzo Avaldi, Paola Bolognesi, Mattea Carmen Castrovilli, Daniele Catone, Marcello Coreno, Fabio Zuccaro, Elisa Bernes, Giovanna Fronzoni, Daniele Toffoli, and Aurora Ponzi

Cite This: J. Phys. Chem. A 2020, 124, 4115–4127 Read Online

ACCESS | Metrics & More | Article Recommendations | Supporting Information

ABSTRACT: The valence and core-level photoelectron spectra of gaseous indole, 2,3-dihydro-7-azaindole, and 3-formylindole have been investigated using VUV and soft X-ray radiation supported by both an ab initio electron propagator and density functional theory calculations. Three methods were used to calculate the outer valence band photoemission spectra: outer valence Green function, partial third order, and renormalized partial third order. While all gave an acceptable description of the valence spectra, the last method yielded very accurate agreement, especially for indole and 3-formylindole. The carbon, nitrogen, and oxygen 1s core-level spectra of these heterocycles were measured and assigned. The double ionization appearance potential for indole has been determined to be 21.8 ± 0.2 eV by C 1s and N 1s Auger photoelectron spectroscopy. Theoretical analysis identifies the doubly ionized states as a band consisting of two overlapping singlet states and one triplet state with dominant configurations corresponding to holes in the two uppermost molecular orbitals. One of the singlet states and the triplet state can be described as consisting largely of a single configuration, but other doubly ionized states are heavily mixed by configuration interactions. This work provides full assignment of the relative binding energies of the core level features and an analysis of the electronic structure of substituted indoles in comparison with the parent indole.

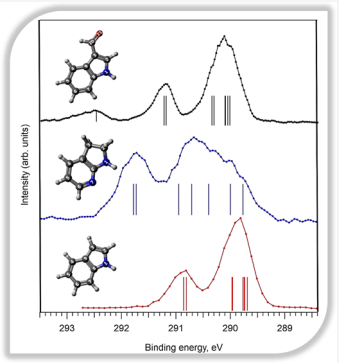

INTRODUCTION

Indole (I), 2,3-dihydro-7-azaindole (7-AI), and 3-formylindole (3-FI) (see Figure 1) heterocycles are prevalent substructures in naturally occurring and synthetic molecules playing key roles in chemistry and biology.[1] Indole derivatives possess unique biological characteristics such as antioxidant, anticancer, antibacterial, antifungal, anti-inflammatory, antiviral, anticonvulsant, and antihypertensive properties among other applications. In addition, indole-based chromophores form the basic building block units of the eumelanin pigments that occur frequently in nature and serve to protect organisms from potentially damaging effects of UV light.[2] 7-AI, whose molecular structure is shown in Figure 1b, has received considerable attention since the corresponding dimer has been recognized as a simple model for the hydrogen-bonded base pairs of DNA and could provide information on the possible role of tautomerism in mutation.[3−5] 3-Formylindole is a heteroarenecarbaldehyde, that is, the hydrogen at position 3 of indole has been replaced by a formyl group (see Figure 1c), and is known as a biologically active metabolite.[6]

Additionally, in recent years, indoles have received increasing attention as coating materials, because they are easily electrografted to surfaces, forming conductive films.[7] Indole-coated surfaces have widespread applications and can

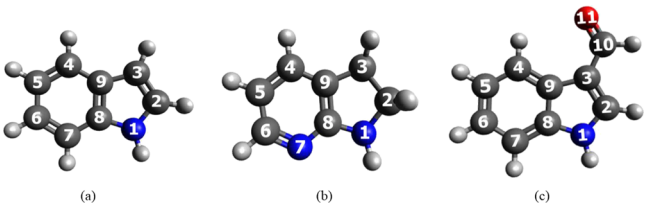

Figure 1. Schematic chemical structures of the investigated indoles: (a) indole (I), (b) 2,3-dihydro-7-azaindole (7-AI), and (c) 3-formylindole with the trans orientation of the formyl group (3-FI). The C (black), N (blue), and O (red) atoms are labeled.

Received: March 27, 2020
Revised: April 24, 2020
Published: April 24, 2020

https://dx.doi.org/10.1021/acs.jpca.0c02719
J. Phys. Chem. A 2020, 124, 4115–4127

be used as selective electrodes sensitive to various cationic and anionic inorganic species, as a biosensor for biological molecules, or as a protection of metallic surfaces against corrosion.[8,9] According to the literature, many intrinsic properties (for example, the polymerization mechanism) of organic heterocycle compounds are masked by their environment or by their interactions with it.[10,11] Thus, gas-phase data provide a better understanding of the properties of indole and its derivatives in the absence of perturbations due to their interactions with different surfaces.

Because of their rich chemistry and biological activity, indoles have been extensively studied using various spectroscopies. Experimental studies of electronic properties of indole and its derivatives have employed optical (including vibrationally and rotationally resolved) methods[12−19] as well as time-resolved ion and photoelectron spectroscopy[20−24] as these powerful techniques probe the properties of greatest interest. Theoretical studies of these heterocycles have been mainly focused on optimization of the structure and calculations of vibrational spectra using the ab initio Hartree−Fock (HF), density functional theory (DFT), and MP2 methods.[25−29]

Recently, the photoinduced structural transformations of indole, 7-azaindole, and 3-formylindole isolated in cryogenic noble-gas matrices were studied by Nowak and co-workers.[30,31] It was found that the tendency of indole and other indole derivatives to undergo hydrogen-atom transfer from N1 to C3 seems to be strongly related with the formation of C3-centered radicals, which facilitate the reattachment of the labile hydrogen atom at this position. The authors[31] have observed that the pattern of photochemical transformations found for 7-AI isolated in solid n-H_2 and irradiated with UV ($\lambda > 270$ nm) light, is significantly different from that observed for the compound trapped in solid Ar. While the C3H tautomer and 7-azaindolyl radical were photogenerated in both environments (solid Ar and solid n-H_2), the N7H tautomer was not photoproduced from 7-AI isolated in solid n-H_2. Additionally, the conformational 1H-*trans* ↔ 1H-*cis* phototransformation by rotation of the aldehyde group in 3-formylindole has been studied as well.[30] It was proposed that the 1H-*trans* isomer of 3-FI is the most populated form of the compound isolated in Ar matrices, whereas the 1H-*cis* isomer could also be populated but with a considerably lower population.

The photoelectron spectrum (PES) of indole was measured many years ago by Eland.[32] Later the PES of indole in the outer valence region was studied with a He I (21.2 eV) source in order to determine whether any correlation between the ionization potential and drug activity exists.[33] Kovać et al. recorded He I PES of 10 different nitrogen-containing heterocycles, and assignment of the results was provided on the basis of molecular orbital calculations.[34] In the late 1980s, multiphoton ionization photoelectron spectroscopy was used in order to obtain information about the adiabatic and vertical ionization potentials of 7-AI in a supersonic jet.[35] Recently, a comprehensive electronic-structure analysis of parental structures of BN indoles (bicyclic aromatic heterocycles in which a 1,3,2-diazaboroline is fused to a benzene ring) in direct comparison to the parent indole was carried out by Chrostowska et al.[36] using a combined UV-PES and computational chemistry approach.

An inner-shell photoionization study of a gas-phase indole was published by Kierspel and co-authors.[37] Detailed photoionization and photofragmentation spectra of indole upon single-photon inner-shell ionization at a photon energy of 420 eV were recorded. This photon energy was chosen so that indole could be locally ionized at its nitrogen or carbon atoms. In addition, electrons and ions were measured in coincidence in a velocity-map-imaging mode to extract 2D and 3D velocity vectors of the charged particles. It was found that the fragmentation channels depend on the ionized electronic states, i.e., the potential energy surfaces, whereas the observed velocities of the fragments are not strongly dependent on these chemical details.[37] However, it appears that up to now experimental evidence concerning the full valence and core electronic structure for derivatives of indole under isolated conditions is still limited. To the best of our knowledge, complete electronic structure investigations obtained by soft X-ray photoemission and near edge X-ray absorption fine-structure (NEXAFS) spectroscopy only exist for gaseous 3-methylindole.[38,39] The valence molecular orbitals and core levels of tryptamine and tryptophol (both contain indole rings but differ in having amino versus hydroxyl terminations of the side chain) in the gas phase have been studied using X-ray photoelectron spectroscopy (XPS) and theoretical methods.[40]

Considering the general importance of these nitrogen-containing heterocycles, an accurate knowledge of their electronic structure becomes crucial. In the present work, we provide a comprehensive electronic structure analysis for two indole derivatives - in direct comparison to the parent indole - by combining valence band (VB) and XPS with theoretical calculations. VB spectra allow us to experimentally determine the ionization energies of molecules that can be correlated to the energies of occupied molecular orbitals, while XPS provides localized ionization of a specific atom, and chemical information about that atom.

EXPERIMENTAL AND THEORETICAL METHODS

Theoretical Methods. Geometry optimizations for the gas-phase molecules were carried out at the DFT B3LYP/aug-cc-pVTZ level by using the Gaussian09 program,[41] and the optimized structures presented in Figure 1 were used for all subsequent calculations. The complete charge density maps of the outermost molecular orbitals (MOs) of I, 7-AI, and 3-FI within the Hartree−Fock/cc-pVTZ model are reported in Figures S1−S3 of the Supporting Information.[42] Note that, in the case of the 3-formylindole molecule, all calculations were performed for its more stable 1H-*trans* (0.0 kJ/mol) conformer rather than the less stable 1H-*cis* (5.1 kJ/mol) conformer.[30]

To a first approximation, the VB ionization spectrum can be described by exploiting Koopmans' theorem (KT). This establishes a direct correlation between the single bands of the spectrum and the MO energies. KT values corresponding to the vertical ionization potential (IP) are reported in Tables S1−S3 of the Supporting Information.[42]

To obtain a more accurate description of the valence spectra, vertical IPs have been calculated with three different ab initio electron propagator (EP) methods. The IPs are obtained as poles of the EP, which in turn correspond to the eigenvalues of a Dyson equation, which must be solved self-consistently.[43] These methods are only applicable in instances where KT provides a reasonable description of initial and final states (quasiparticle approximation or an orbital picture of ionization), and the Dyson orbitals are therefore proportional to the HF orbitals. Diagonal approximations usually fail in the presence of strong relaxation effects and cannot describe the strong redistribution of intensity from the main lines to satellite states, which is usually observed in inner-valence

https://dx.doi.org/10.1021/acs.jpca.0c02719
J. Phys. Chem. A 2020, 124, 4115−4127

Table 1. Experimental and Calculated Outer Valence Band Binding Energies of Indole, 2,3-Dihydro-7-azaindole, and 3-Formylindole

compounds	experimental BEs (eV), present work, ±0.1 eV		calculated BEs (eV) using the P3+/cc-pVTZ approach / molecular orbital (type)	published BEs (eV)[33,35,36]
indole		7.72[a]		
	7.77 (shoulder)	7.76[a] (shoulder)		7.75[33]
	7.90	7.90[a]	7.911 / 5a″ (π_1) (HOMO)	7.92;[33] 7.9[36]
	8.07 (shoulder)	8.05[a]		8.08[33]
	8.32	8.35[a]	8.245 / 4a″ (π_2)	8.37;[33] 8.5[36]
	8.42 (shoulder)			
	9.82		9.881 / 3a″ (π_3)	9.83;[33] 9.9[36]
	10.97		11.285 / 2a″ (π_4)	11.02;[33] 11.05[36]
	11.55		11.677 / 26a′ (σ)	11.45[36]
	12.20		12.270 / 25a′ (σ)	12.25[36]
	12.62 (H_2O)			
	13.02		13.291 / 24a′ (σ)	13.00[36]
	13.80		13.878 / 23a′ (σ)	
			13.662 / 1a″ (π)	
	14.25		14.371 / 22a′ (σ)	
			14.519 / 21a′ (σ)	
	15.30		15.583 / 20a′ (σ)	
	15.80		15.880 / 19a′ (σ)	
	17.00		17.482 / 18a′ (σ)	
	18.52			
	19.25			
2,3-dihydro-7-azaindole	7.92		7.916 / 32a (π) (HOMO)	8.11[35]
	9.42 (shoulder)		9.382 / 30a (n_N)	
	9.81		9.823 / 31a (π)	
	10.56		10.540 / 29a (π)	
	12.15		12.303 / 28a (σ)	
			13.035 / 27a (σ)	
	13.23 (broad)		13.157 / 26a (σ)	
			13.423 / 25a (σ)	
			13.517 / 24a (σ)	
			13.581 / 23a (σ)	
	14.58		14.576/ 22a (σ)	
	15.30		15.388 / 21a (σ)	
	15.63		15.945 / 20a (σ)	
			16.345 / 19a (σ)	
	16.98		17.365 / 18a (σ)	
	19.20 (broad)			
3-formylindole	8.15			
	8.30		8.354 / 6a″ (π) (HOMO)	
	8.72		8.684 / 5a″ (π)	
	9.11 (shoulder)			
	9.23		9.339 /32a′ (n_O)	
	10.06		10.105 / 4a″ (π)	
	11.40		11.663 /3a″ (π)	
	11.90		12.035 / 31a′ (σ)	
	12.52		12.485 / 30a′ (σ)	
	13.35		13.012 / 2a″ (π)	
			13.618 / 29a′ (σ)	
	14.23		14.247 / 28a′ (σ)	
			14.566 / 27a′ (σ)	
			14.308 / 1a″ (π)	
			14.514 / 26a′ (σ)	
			14.851 / 25a′ (σ)	
	15.50		15.775 / 24a′ (σ)	
			16.342 / 23a′ (σ)	
	17.30 (broad)		17.637 / 22a′ (σ)	
	18.70		18.184 / 21a′ (σ)	

[a]High resolution data for the first two low-energy bands of indole.

https://dx.doi.org/10.1021/acs.jpca.0c02719
J. Phys. Chem. A 2020, 124, 4115−4127

ionizations. This is reflected in computed pole strengths (PS) smaller than 0.85.[44] EP methods used in this work include the outer valence Green function (OVGF),[43,45] partial third order (P3),[46] and renormalized partial third order (P3+)[47] methods, as implemented in Gaussian 09 in combination with the cc-pVTZ basis set. As mentioned above, these methods are of sufficient quality to yield reasonable agreement with experimental IPs in instances where the breakdown of the orbital picture of ionization does not occur (as seen from the computed pole strengths and also reported in the Supporting Information[42]). Several studies demonstrate that, within the diagonal self-energy approximation, P3+ combined with a basis set of triple-zeta quality represents the best compromise between accuracy and computational efficiency (i.e., see ref 48).

Regarding the core region, the C 1s, N 1s, and O 1s photoelectron spectra were calculated at the DFT level[49] with the hybrid B3LYP[50] and the generalized gradient approximation (GGA) PW86x Perdew[51] exchange correlation (xc) potentials and with the Amsterdam density functional (ADF) program.[52] The IPs were computed with the delta Kohn−Sham (Δ-KS) scheme, namely, as differences between the KS solution in the ground state and ionic state. This calculation allows full relaxation of the ionized core hole within a spin-polarized unrestricted scheme.

Experimental Methods. Indole, 7-AI, and 3-FI were purchased from Sigma-Aldrich in the form of crystalline powder with a minimum purity of 99% and used without further purification. The samples were introduced into the system via an effusive needle source at room temperature (I and 7-AI) or evaporated from a crucible at a temperature of 350 K (3-FI) and a background pressure of 1 to 7 × 10^{-7} mbar. During the experiment, the sample quality was periodically monitored by valence band photoemission and photoionization mass spectroscopy.

The photoemission spectra were collected at the Gas Phase Photoemission and Circular Polarization beamlines at Elettra (Trieste, Italy).[53,54] The high-resolution C 1s, N 1s, and O 1s XPS and valence band spectra were measured using a VG-220i hemispherical electron energy analyzer. The analyzer was mounted in the plane perpendicular to the photon propagation direction and at an angle of 54.7° with respect to the electric vector of the light. In this geometry, the axis of the analyzer is set at the pseudo magic angle, and so measurements are insensitive to the photoelectron asymmetry β parameter. A homemade ion time-of-flight (TOF) mass spectrometer was mounted in the same chamber, facing the analyzer. This spectrometer configuration was successfully used to study various biological molecules in previous experiments.[55] Recently, the performance of this instrument was improved by replacing the six-channel electron multiplier detector unit of the analyzer by a rectangular microchannel plate detector[56] coupled to a 2D time delay-line anode developed by the Elettra detector laboratory.[57,58] The current detector covers ∼12% of the selected pass energy in a single exposure and thus requires shorter acquisition times.

In addition, the previous rectangular electron multipliers with a 2 mm opening in the dispersive direction acted also as exit slits. The analyzer resolution for a given pass energy is now governed mainly by the analyzer entrance lens optics as the detector acts as a virtual exit slit, adjustable simply by choosing the region to be integrated. In practice, under standard operation conditions, the kinetic energy resolution for pass energies above 10 eV was improved by ∼25% with respect to the previous detector. The replacement of the detector has significantly improved the performance of the setup in energy-analyzed PEPICO experiments, which will be the subject of a separate publication.[59]

Valence spectra of the indoles were recorded with an incident photon energy of 60 eV; they are consistent with those previously measured with a He I (21.2 eV) source[32−36] apart from differences in relative peak intensity due to cross-sectional differences at the two photon energies. The binding energy (BE) scale for valence band spectra was calibrated using H_2O (from residual gas).[60] The C 1s, N 1s, and O 1s core photoemission spectra were taken at 385, 495, and 628 eV of photon energy, respectively, and they were calibrated according to the well-known references of CO_2 BE $(C(1s)^{-1}$ at 297.7 eV, $O(1s)^{-1}$ at 541.3 eV,[61,62] and N_2 $(N(1s)^{-1}$ at 409.9 eV).[63] The spectra were measured with a total resolution (photons + analyzer) of 0.20, 0.32, 0.46, and 0.53 eV at photon energies of 60, 385, 495, and 628 eV, respectively. At these photon energies, the kinetic energy of the photoelectrons is such that the effects due to post collisional interaction (PCI) can be neglected in the data analysis. Additionally, VB spectra for indole were taken at higher resolution of 50 meV in order to determine more accurately ionization potentials of the first two low-energy bands associated with its highest occupied molecular orbitals (HOMO and HOMO-1). The changes in transmission of the analyzer over the relatively small range of the photoelectron spectra shown were neglected.

RESULTS AND DISCUSSION

Valence Photoemission Spectra. For all three molecules, we performed OVGF, P3, and P3+ calculations in order to identify the most accurate EP method for reproducing the valence photoemission spectra. The complete list of calculated energies, together with the corresponding pole strengths, is given in the Supporting Information.[42] The assignments of the observed features of the outer valence band based on the P3+ calculations are summarized in Table 1. Additionally, the present data have been compared with previously reported experimental values obtained using He I radiation.[33,35,36]

Before describing our photoelectron spectra, we note that the three studied heterocycles have chemical differences (see Figure 1). For example, indole is a benzo-indole, a planar compound, and 7-azaindole is a non-planer compound due to the sp^3 hybridization of C2 and C3 atoms in the pentagonal ring. The pair differs in both the hexagon and pentagonal rings. Indole and 3-formylindole are both benzo-indoles that differ by the 3-formyl group in the pentagonal ring, but the latter has both *trans*- and *cis*-conformers, which are detectable.[30] Hence, the difference in their chemical structure will influence the shape and peak positions of the measured PES spectra.

The photoelectron spectrum of indole exhibits a low-energy band at 7.90 eV, which is associated with its highest occupied molecular orbital (HOMO) of π symmetry (5a″). The next three bands, appearing at 8.32, 9.82, and 10.97 eV, correspond to the 4a″, 3a″, and 2a″ MOs, respectively. These MOs also have π character and are delocalized on the indole ring (see Figure 3). Our assignment is consistent with the available valence photoemission spectra for indole;[33,36] moreover, the ionization energies of the lowest MOs are well reproduced by the present P3+ calculations (see Table 1). The first three peaks are mostly found at the predicted energies, while for the fourth ionization (2a″), we find a discrepancy of 0.3 eV with

https://dx.doi.org/10.1021/acs.jpca.0c02719
J. Phys. Chem. A 2020, 124, 4115−4127

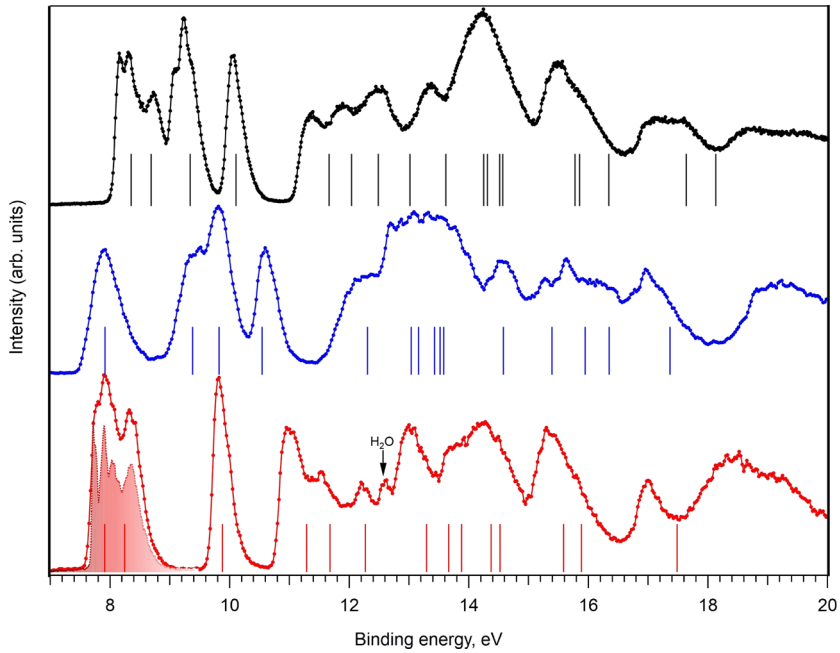

Figure 2. Dotted lines: valence-band photoelectron spectra of indole (bottom curve, red), 2,3-dihydro-7-azaindole (center curve, blue), and 3-formylindole (top curve, black) at a photon energy of 60 eV. Shaded spectrum: higher-resolution valence band spectrum of indole. Bars: calculated BEs for each compound using the P3+ cc-pVTZ model.

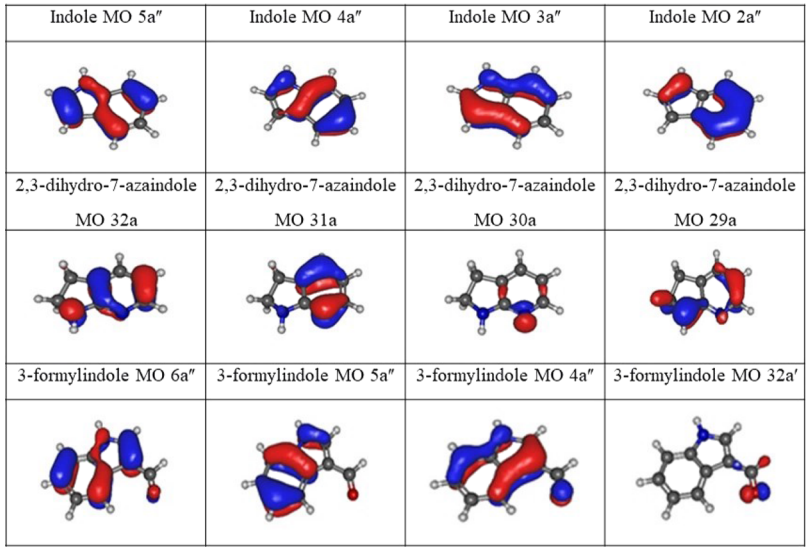

Figure 3. Charge density maps of the outermost molecular orbitals of indole, 2,3-dihydro-7-azaindole, and 3-formylindole.

respect to the experimental value. The computed low PS value (0.815) for this MO indicates however a likely breakdown of the quasi-particle picture of ionization (see Table S1 of the Supporting Information).[42]

The higher resolution VB spectrum of indole (see Figure 2, shaded spectrum) consists of several bands at low IPs accompanied by vibrational splitting of π_1 (7.72, 7.76, and 7.90 eV) and π_2 (8.05 and 8.35 eV) orbitals. This spectrum is in good agreement with that of Domelsmith and co-workers[33] with BEs of 7.75, 7.92, 8.08, and 8.37 eV. The indole structure consists of fused pyrrole and benzene rings (see Figure 1). For comparison, pyrrole has its first two valence orbitals at 8.2 and 9.2 eV, while those of benzene are at 9.4 and 11.8 eV.[64]

The substitution of one carbon atom in the benzene ring of indole by nitrogen (see Figure 1b) forms 2,3-dihydro-7-azaindole (7-AI), which has a different photoemission spectrum. Similar to indole, the first broad band located at 7.92 eV was assigned to the HOMO. The vertical ionization potential found here for 7-AI is slightly lower (~0.2 eV) than that published by Fuke et al.[35] The second feature with maxima at 9.42 and 9.81 eV is close to the assignment found for the lowest IP of pyridine, 9.6 eV.[60,65] The first region of the VB ionization in pyridine has been attributed to both π- and n-orbital ionization, and photoemission spectra support the view that there are two overlapping bands. The comparison of our experimental and computational data shows that the replacement of one carbon atom in indole by nitrogen does not result in significant changes in the energy levels of the corresponding HOMOs. According to our calculations, the features in the valence photoemission spectrum of the 7-AI

https://dx.doi.org/10.1021/acs.jpca.0c02719
J. Phys. Chem. A 2020, 124, 4115−4127

molecule at 9.81 and 10.56 eV are assigned to the MO with π symmetry, while the shoulder at 9.42 eV is due to the nitrogen heteroatom lone pair (see Figure 3). In the case of 7-AI, EP methods produce a different ordering of the cationic states with respect to that of the KT. In particular, ionization energies related to the π (31a) and n (30a) MOs are reversed. This shows that, for the cases of nitrogen-containing heterocycles, EP corrections to Koopmans' results are essential to produce correct assignments of photoelectron spectra.[66,67] In fact, correlation and relaxation effects are generally much more relevant for hole states with dominant contributions from nonbonding, nitrogen-centered functions than for delocalized π MOs.

The first photoelectron peak of 3-FI is split into peaks at 8.15 and 8.30 eV and corresponds to the HOMO ionization. From the computed relative energies of 1H-*trans* and 1H-*cis* isomers of 3-FI, the relative Boltzmann populations of these two forms in the gas phase at 350 K were estimated as ∼85% 1H-*trans* and ∼15% 1H-*cis*.[30] Hence, the splitting of the first maximum could be due to the presence of different conformers.

The next bands at 8.72 and 10.06 eV are assigned to MOs (HOMO-1 and HOMO-2) of π symmetry. The asymmetric feature at 9.23 eV is due to the ionization of the 32a′ MO, which is mostly located on the oxygen heteroatom lone pair (see Figure 3). This assignment is in good agreement with already published valence band photoemission data for tryptophol, which also contains an indole ring but differs in having a flexible ethanolic side chain.[40]

As for 3-FI, the KT results are quantitatively inadequate, and they fail to predict the right order of final states. The correct ordering is retained by using EP methods, which consider both electron correlation and orbital relaxation effects, particularly relevant for final states with lone pair holes. However, while, in the case of 7-AI, both OVGF and P3+ methods correctly reproduce the band related to the ionization from the lone-pair, for the 3-FI molecule, P3+ results agree with the experiment better than those from OVGF and P3 (see the Supporting Information, Tables S1−S3).[42] In particular, OVGF overestimates the energy related to the lone-pair band by 0.52 eV, while both P3 and P3+ properly predict that energy, providing results in good agreement with the experimental data (see Table S3, Supporting Information).[42] Moreover, a comparison of the computed PS for the valence ionization of 7-AI and 3-FI reveals that the latter is a more challenging system for all diagonal EP approximations: with the exception of the outermost HOMO, HOMO-1, and HOMO-2 ionizations of π-type MOs, for all other π MOs, the low values of the corresponding PS indicates the importance of orbital relaxation effects. In fact, significant relaxation effects are anticipated for all ionization energies above 18 eV (see Table S3, Supporting Information).[42]

Core Level Photoemission. The C 1s, N 1s, and O 1s XPS experimental and theoretical photoemission spectra of the samples are shown in Figures 4 and 5 and Figure S4 of the Supporting Information (O 1s XPS)[42] and summarized in Table 2. Experimentally derived BEs are compared with theoretical BEs computed by using the hybrid B3LYP xc potential. The assignment of the spectral features is rationalized considering that core level BEs are very sensitive to the chemical environment of the ionized atomic site in terms of both electron density and electronic relaxation. Starting with I, the carbon core-level spectrum (see Figure 4)

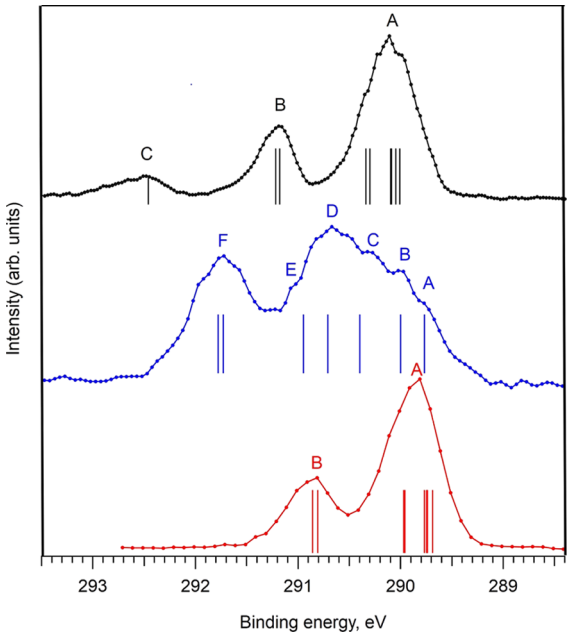

Figure 4. C 1s photoemission spectra of indole (bottom curve, red), 2,3-dihydro-7-azaindole (center curve, blue) and 3-formylindole (top curve, black). Dotted lines: experimental data. Bars: theoretical data computed by using the hybrid B3LYP xc potential. Calculated BEs were shifted by +0.2, +0.15, and +0.1 eV for indole, 2,3-dihydro-7-azaindole, and 3-formylindole, respectively.

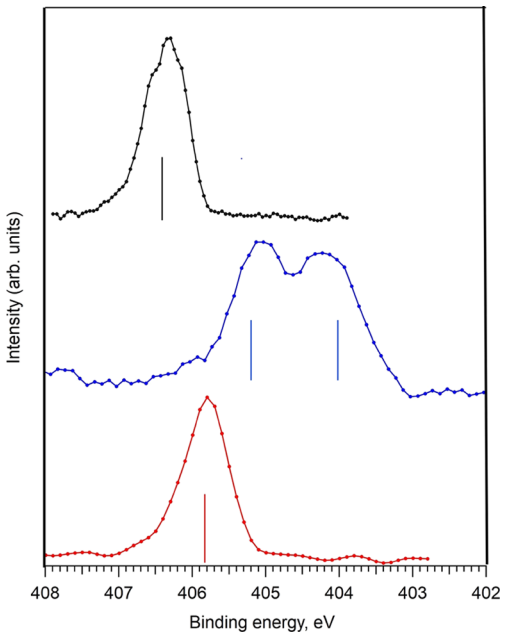

Figure 5. N 1s photoemission spectra of indole (bottom curve, red), 2,3-dihydro-7-azaindole (center curve, blue) and 3-formylindole (top curve, black). Dotted lines: experimental data. Bars: theoretical data computed by using the hybrid B3LYPxc potential. Calculated BEs were shifted by +0.35 eV for all three indoles.

shows two distinct features (labeled A and B) centered at 289.89 and 290.86 eV with an integrated intensity ratio of 6:2. Indole is formed by the fusion of a pyrrole ring to the benzene ring at the C9═C8 position (see Figure 1a). Our calculations show that all the carbon atoms not bonded to nitrogen contribute to the strongest peak A of the photoemission

https://dx.doi.org/10.1021/acs.jpca.0c02719
J. Phys. Chem. A 2020, 124, 4115−4127

Table 2. C, N, and O 1s Experimental and Calculated BEs for Indole, 2,3-Dihydro-7-azaindole, and 3-Formylindole

molecule/ core level	experimental BEs (eV) ± 0.1 eV/feature	calculated BEs (eV) ± 0.1 eV, DFT: B3LYPxc/PW86x/Assignment
indole		
C 1s	289.89/A	289.49/289.86/C5
		289.54/289.93/C3
		289.55/289.91/C6
		289.57/289.93/C4
		289.76/290.16/C9
		289.77/290.15/C7
	290.86/B	290.61/290.94/C2
		290.66/291.01/C8
N 1s	405.82	405.45/406.13/N1
2,3-dihydro-7-azaindole		
C 1s	289.77/A	289.62/289.99/C5
	290.00/B	289.85/290.26/C9
	290.27/C	290.25/290.55/C4
	290.67/D	290.56/290.84/C6
	291.02/E	290.80/291.20/C3
	291.72/F	291.58/291.95/C2
		291.63/291.87/C8
	404.23	403.56/404.17/N7
N 1s	405.03	404.69/405.35/N1
3-formylindole		
C 1s	290.25/A	289.91/290.34/C5
		289.95/290.37/C6
		289.99/290.42/C4
		290.00/290.45/C3
		290.20/290.63/C7
		290.24/290.67/C9
	291.33/B	291.08/291.41/C2
		291.12/291.51/C8
	292.65/C	292.36/292.45/C10
N 1s	406.36	406.04/406.71/N1
O 1s	536.84	535.89/536.76/O11

spectrum, while peak B is due to the C2 and C8 carbons bonded to the N atom, as summarized in Table 2. Their higher BE values are due to their higher electrostatic potential with respect to the other C sites. The observed C 1s BEs are in good agreement with previously published data for 3-methylindole,[39] tryptophol,[40] tryptamine,[40] benzene, and pyrrole.[64] The BE of the benzene C ls level was found to be 290.20 eV[64] and it is about 0.3 eV higher than the measured energy of peak A. The small shift in BE can be attributed to the final-state screening, because indole is larger and more polarizable than the benzene ring.

The C 1s spectra for I and 3-FI are, as expected, quite similar, given that the molecules differ by one hydrogen atom being replaced by a formyl group (see Figure 1). The area ratios of peaks A:B:C in the spectrum of 3-FI are 6:2:1. We notice that the position of peaks A and B is shifted to higher BEs (by about 0.30 eV) on going from I to 3-FI, due to the presence of the formyl group in 3-FI. In the C 1s XPS spectrum of 3-FI, the broad peak C at 292.65 eV is assigned to the ionization of the carbon atom bonded to the electronegative oxygen atom which causes an increase of the electrostatic potential at the carbon nucleus (see Figure 4). As in the case of indole, tryptophol, tryptamine and 3-methylindole, the most pronounced feature A, centered at 290.25 eV in the carbon core level spectrum of 3-FI, is due to the aromatic ring carbons[39,40,64] which are not directly bonded to N, while feature B is associated with ionization from C8 and C2 (see Table 2).

The experimental full widths at half maximum of the most intense features A (see Figure 4) in the C 1s spectra of indole and 3-formylindole, are about 0.89 and 0.84 eV, respectively. Assuming Gaussian peak shapes and considering the total experimental resolution of 0.32 eV, the observed widths derived are 0.79 and 0.74 eV. The number of closely spaced electronic states and their vibrational envelopes hamper a better definition of the structure, even for improved experimental resolution.

7-AI contains seven carbon atoms, and wide asymmetric peaks are seen in its C 1s photoemission spectrum (see Figure 4). The low BE feature of the C 1s XPS spectrum of 7AI is noticeably broader than for the other two indoles, and shows five well resolved shoulders (A-E) lying in the range 289−291 eV (see Figure 4). The distinct shifts of the carbon 1s BEs of 2,3-dihydro-7-azaindole are due to the different chemical environment and could be characterized as a superposition of carbon atoms from the pyridine and pyrrole rings. The experimental C 1s BEs for pyridine were found to be 290.9 eV, 290.6 eV and 290.2 eV for (C2 = C6), (C4), and (C3 = C5) core holes, respectively.[68,69] For pyrrole, two carbon core-electron BEs at 290.8 eV (C2 = C5) and 289.8 eV (C3 = C4) have been published by Gelius et al.[64] It is interesting to note the manner in which C 1s BEs values for the 7-AI molecule interchange with respect to the position of the carbon atom in a ring system such as pyridine, in which the lowest carbon ionization values were obtained for the C9 and C5 atoms located as nearest-neighbors to the (N7) atom (see Table 2). The same trend was observed for various carbon−nitrogen molecules by Snis et al.[68] The highest BE feature F at 291.72 eV has been assigned as for indole and 3-formylindole, and is due to the two carbon atoms (C2 and C8) which are nearest-neighbors of nitrogen (N1) in the pyrrole ring (see Figure 1). The values are about 0.86 and 0.39 eV higher than the energy of the same carbons in the indole and 3-FI molecules, respectively (see Table 2). This can be explained by considering the electronegativity of the neighbouring atoms. For the case of 7-AI, the electronegative N-atom directly bonded to C8 produces a decrease of the electron density around the C-atom and therefore an increase of the binding energy. Such an effect is reduced in the case of 3-FI, as the electronegative oxygen atom is not directly bonded to the considered C atoms.

The N 1s photoemission spectra of indole and 3-FI present broad single features at 405.82 and 406.36 eV, respectively (see Figure 5). In both cases the peak derives from the same chemical environment and is due to the nitrogen atom (N1) in the pyrrole ring. The experimental N 1s BE for pyrrole was determined to be 406.1 eV,[64] and it is approximately 0.3 eV higher than the value obtained for indole and lower than those measured for 3-methylindole. The BE of the indole nitrogen matches well the already published values for 3-methylindole (405.7 eV),[39] tryptophol, and tryptamine (405.73 eV).[40]

The N 1s spectra of indole and 3-formylindole both show asymmetric peaks, a shape which has been attributed to Franck−Condon effects.[39] The experimental fitted widths are about 1.03 and 0.94 eV for indole and 3-FI, respectively. Taking into account the experimental resolution, this implies intrinsic widths of 0.82 and 0.73 eV, similar to the values obtained from the C 1s spectra.

https://dx.doi.org/10.1021/acs.jpca.0c02719
J. Phys. Chem. A 2020, 124, 4115−4127

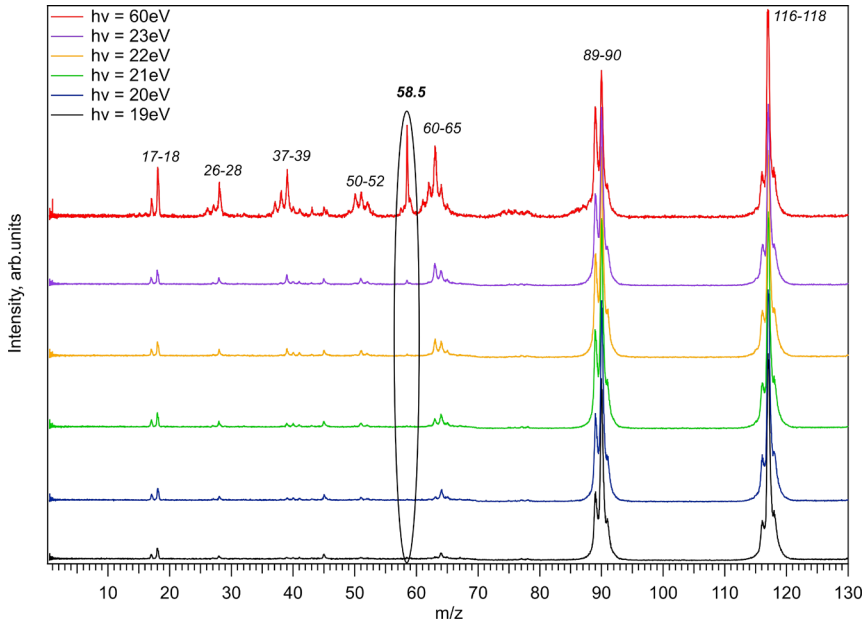

Figure 6. Mass spectra of indole as a function of photon energy.

In 7-AI, two nitrogen atoms are present, and two peaks are observed in the experimental spectrum at 404.23 and 405.03 eV (see Figure 5). The difference in energy between these features is 0.8 eV, slightly lower than that predicted by theoretical calculation (~1.15 eV) (see Table 2). The peak at higher BE corresponds to the N1 atom in the pyrrole ring, which has the same pattern as that found for indole, 3-formylindole, 3-methylindole, tryptophol, and tryptamine measured under similar experimental conditions. The lower-energy peak at 404.23 eV is assigned to the N atom of the pyridine ring. Their relative positions can be understood by simple arguments based on the different electron shielding effects on the two N positions. The experimental position of the N 1s peak corresponding to the ionization of the N1 atom for 7-AI is approximately 0.8 and 1.3 eV lower with respect to the single features observed for I and 3-FI, respectively. The closest calculated N 1s BEs found for pyridine are 404.69 eV[68] and 404.76 eV,[69] approximately 0.5 eV higher than the N7 atom energy in 7-AI. Also, experimental values of nitrogen core-electron BEs of pyridine show a shift, which is approximately 0.7 eV higher[69] with respect to the value measured in the present work. It is well known that, in the case of organic heterocycles, the ionization energy decreases with the increasing size of the system.[68]

The computed and measured O 1s core level spectra of 3-formylindole are displayed in Figure S4 (see the Supporting Information),[42] while the corresponding BEs are summarized in Table 2. There was no effect of the molecular conformation observed in the experimental O 1s spectrum of 3-FI. The intense peak at 536.84 eV was assigned to the oxygen atom of the formyl group in the molecule. In the case of 3-FI the O 1s BE is lower than for tryptophan and tryptophol, which contain the indole structure and an additional carboxyl or hydroxyl group.[39,40] Based on its energy, we attribute the wide asymmetric peak at 539.80 eV to water present in the sample and/or the experimental chamber.[70]

Doubly Charged Ions of Indole. Mass spectrometry has provided a large amount of data for doubly charged ions (dications).[71−73] The minimum energy required to form the doubly charged ion is denoted variously in the literature as the double ionization potential (DIP), double ionization energy (DIE), or appearance potential (AP). In this section, we report data for the double ionization of indole.

The parent ion (M^+) of indole m/z = 117 dominates the mass spectrum at all photon energies (see Figure 6). It has been shown that, for aromatic heterocyclic fused-ring compounds containing more than one nitrogen atom, in most cases, the dominant fragmentation reaction of M^+ involves expulsion of HCN° (or HNC°) neutral species (m = 27).[73] Consistent with this, at all the photon energies used, the next most intense pair of masses after the parent ion are at m/z = 90 and m/z = 89 corresponding to $C_7H_6^+$ and $C_7H_5^+$ fragments. The very weak signal at m/z = 58.5 in the spectrum measured at $h\nu$ = 22 eV is due to the formation of the dication. As the photon energy increases, the signal of the doubly charged ion becomes more pronounced (see Figure 6, $h\nu$ = 60 eV). In general, the probability for double ionization is always lower than that of the single ionization. Note that our photofragmentation spectra of indole are in good agreement with those measured by electron impact at 70 eV.[65] Additionally, fragmentation reactions of both metastable and collisionally activated dications, formed by electron impact ionization of 25 polycyclic aromatic compounds have been investigated in detail by Perreault et al.[73] Their results have been interpreted on the basis of mechanistic models based on the competition between charge-separation and neutral-expulsion reactions and on variations in the diradical character with increasing molecular size and nitrogen content of these molecular dications.

To estimate the appearance potential of the doubly charged ion of indole, we chose Auger electron spectroscopy[74], as the final states of this process are doubly charged. The subtraction of the Auger electron energy from the energy of the initial hole state gives the energy of the state of the ion.[74] The C-Auger spectrum of I measured here shows the first peak centered at a BE of approximately 21.8 eV, which corresponds to its lowest DIE (see Figure 7). This value is consistent with the position of the first wide band presented in the N-Auger spectrum of

https://dx.doi.org/10.1021/acs.jpca.0c02719
J. Phys. Chem. A 2020, 124, 4115−4127

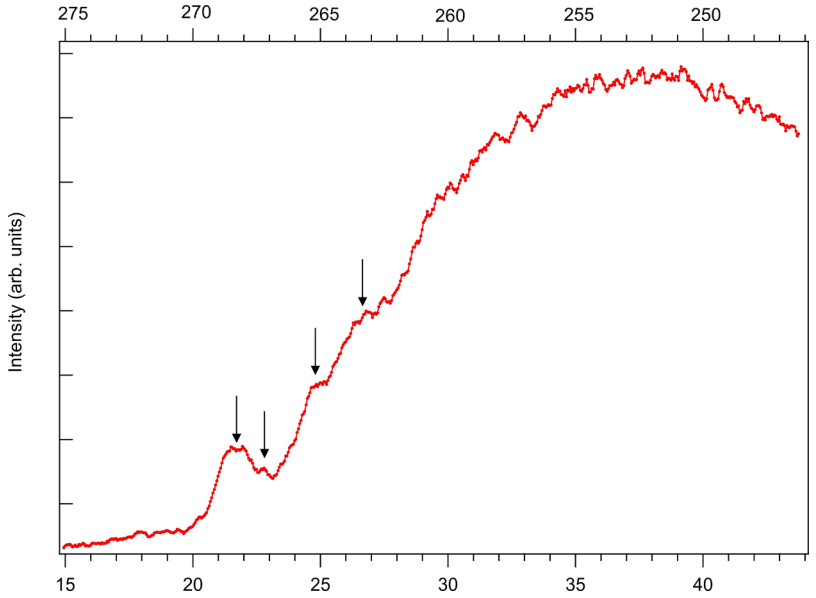

Figure 7. C-Auger spectrum of indole measured at a photon energy of 350 eV.

indole (see the Supporting Information, Figure S5) as well as with our TOF spectra as a function of photon energies (Figure 6). It is not surprising that the present C- and N-Auger spectra of indole have broad structures. This broadening includes the finite line width of the XPS, the vibrational distributions of the core-hole states and the final states, the core-hole lifetime, and also the analyzer resolution. Note that the energy scales of the C- and N-Auger spectra in Figure 7 and Figure S5 (Supporting Information) have been calibrated with respect to CO_2[75] and N_2[76] and the experimentally found BE values 289.89 and 405.82 eV for carbon and nitrogen core-level photoemission spectra of indole, respectively (see Table 2).

In order to understand which orbitals/states of indole are involved in the formation of doubly charged ions, we have performed calculations at the CASSCF/MRCI (complete active space self-consistent field/multi-reference internally contracted configuration interaction) level of theory[77] with the ANO-VT-TZ basis, and these data are summarized in Table S4 of the Supporting Information. All calculations were performed by using the MOLPRO package.[78] In detail, the CASSCF energies were obtained by averaging over the four lowest singlet states and one triplet state with an active space including eight active electrons for the neutral state and six active electrons for the doubly ionized states in six active orbitals (see the Supporting Information, Figures S6 and S7). Although all the calculated states of the doubly charged molecule have mixed configurations, they are mainly dominated by the contribution of one of the reference CI configurations (see Supporting Information, Table S4).[42]

As mentioned above, there are few singlets and one triplet state relatively close in energy (see the Supporting Information, Table S4 and Figures S6 and S7) that could participate in the dication formation. Our calculations show that the first two states ($1^1A'$ and $2^1A'$) are separated by 0.5 eV, while the third state ($3^1A'$) is 1.5 eV higher. As we do not calculate the intensities, the peak shape is difficult to predict. The calculations also show that the next state ($4^1A'$) is much higher in energy, so it would seem that we see the decay to the lowest states for C and for N (see the Supporting Information, Table S4).[42] Note that the lowest triplet state ($1^3A'$) is energetically near (0.18 eV) the lowest singlet state ($1^1A'$) (see the Supporting Information, Table S4). One can assign "dominant configurations" to the lowest states, and we consider holes in the HOMO and HOMO-1. According to Figure 3, these molecular orbitals (5a″ and 4a″) extend over the whole molecule, including the nitrogen atom. Hence, the first wide peak in the N-Auger spectrum (see the Supporting Information, Figure S5) is most likely due to the lowest dication state of indole. The same is true for the C-Auger spectrum (see Figure 7), but things are more complicated here since the molecule has many carbon atoms. The C 1s photoemission spectra of indole show two peaks: one having contributions of C2 and C8 (bound to the nitrogen) at 290.86 eV and the other at 289.89 eV with contributions from all other carbons (see Table 2 and Figure 4). For the lowest dicationic state, this implies that at least two peaks separated by ∼1 eV should be observed in the C-Auger spectrum of indole. In Figure 7, one can see a small shoulder at 22.8 eV, which may tentatively be assigned to this process. From Figure 3, it appears that the two outermost orbitals (MO 5a″ and MO 4a″) extend over C2 and C8 atoms but also over most of the other carbon atoms complicating the final interpretation. Therefore, one could assume that the first observed structure in the C-Auger spectrum is at an energy consistent with a decay from some of the (not nitrogen neighbor) ring carbons to the lowest state of the doubly charged ion. Additionally, our mass spectra are also consistent with the energy obtained from the Auger spectra, showing that the dication is stable on the timescale of our experiment (hundreds of nanoseconds).

Other weak shoulders around 24.84 and 26.78 eV have been observed as well in the C-Auger spectrum of indole. Since no prior experimental and theoretical studies of the double ionization of indoles exist in the literature, we can only compare our data with that of other aromatic compounds (see Table 3).[72,79,80] Dication appearance potentials for aromatic molecules containing a double ring structure (such as indole, quinoline, and azulene) are lower than those having a single-ring structure (benzene, pyridine and pyrimidine). It is certainly possible to predict double ionization appearance potentials from single ionization energies using some empirical

https://dx.doi.org/10.1021/acs.jpca.0c02719
J. Phys. Chem. A 2020, 124, 4115−4127

Table 3. Double Ionization Appearance Potentials of Some Aromatic Molecules

molecule/published data	first peak (DIE) (eV)	other peaks/shoulders
indole (present work)	21.8 ± 0.2	22.8, 24.84, 26.78
pyridine[72]	25.1	from 25.6 to 32.0
pyrimidine[79]	25.4	from 27.61 to 32.16
quinoline[70]	22.4	23.2, 26
benzene[80]	24.65	from 26 to 31
azulene[80]	20.2	21.3, 22.3

equations, provided that one knows the distance between the final charges of the molecule.[72,81] However, this information is often lacking; therefore, this empirical approach is presently of little practical use.

CONCLUSIONS

The core and valence photoemission spectra of three biologically important compounds, namely, indole, 2,3-dihydro-7-azaindole, and 3-formylindole, have been studied in the gas phase using X-ray photoelectron spectroscopy (XPS) and quantum-chemistry calculations. Comprehensive information about the electronic structure and, in particular, the occupied molecular orbitals, has been acquired. The high-resolution spectrum for the inner valence region of indole has been reported, and several bands due to the vibrational splitting of its HOMO and HOMO-1 have been defined. The appearance potential of the doubly charged ion of indole has been determined to be 21.8 ± 0.2 eV by using Auger electron spectroscopy. The carbon, nitrogen, and oxygen 1s photoemission spectra for all three investigated molecules have been assigned. Additionally, calculations presented in this paper are in good agreement with the relative BEs of the core level features observed in the experimental photoemission results. By comparing our data with previously published results, we conclude that the rotation of the formyl group attached in 3-FI to the C3 atom was weak and did not show detectible chemical shifts in the core-level spectra of this molecule.

ASSOCIATED CONTENT

Supporting Information

The Supporting Information is available free of charge at https://pubs.acs.org/doi/10.1021/acs.jpca.0c02719.

Complete list of calculated energies together with the corresponding pole strengths for indole, 2,3-dihydro-7-azaindole, and 3-formylindole; full plot HF/cc-pVTZ orbitals for three nitrogen-containing heterocycles; O 1s photoemission spectrum of 3-formylindole and N-Auger spectrum of indole; and calculated double ionization energy values for the indole molecule (PDF)

AUTHOR INFORMATION

Corresponding Author

Oksana Plekan − *Elettra-Sincrotrone Trieste S.C.p.A., 34149 Trieste, Italy;* orcid.org/0000-0002-4692-7018; Email: oksana.plekan@elettra.eu

Authors

Hanan Sa'adeh − *Elettra-Sincrotrone Trieste S.C.p.A., 34149 Trieste, Italy; Department of Physics, The University of Jordan, Amman 11942, Jordan;* orcid.org/0000-0002-2568-5507

Alessandra Ciavardini − *CERIC-ERIC, 34149 Trieste, Italy*

Carlo Callegari − *Elettra-Sincrotrone Trieste S.C.p.A., 34149 Trieste, Italy*

Giuseppe Cautero − *Elettra-Sincrotrone Trieste S.C.p.A., 34149 Trieste, Italy*

Carlo Dri − *Elettra-Sincrotrone Trieste S.C.p.A., 34149 Trieste, Italy; IOM-CNR Laboratorio TASC, 34149 Trieste, Italy;* orcid.org/0000-0001-9040-5746

Michele Di Fraia − *Elettra-Sincrotrone Trieste S.C.p.A., 34149 Trieste, Italy*

Kevin C. Prince − *Elettra-Sincrotrone Trieste S.C.p.A., 34149 Trieste, Italy; Centre for Translational Atomaterials, Swinburne University of Technology, Melbourne 3122, Australia*

Robert Richter − *Elettra-Sincrotrone Trieste S.C.p.A., 34149 Trieste, Italy*

Rudi Sergo − *Elettra-Sincrotrone Trieste S.C.p.A., 34149 Trieste, Italy*

Luigi Stebel − *Elettra-Sincrotrone Trieste S.C.p.A., 34149 Trieste, Italy*

Michele Devetta − *Istituto di Fotonica e Nanotecnologie, CNR, 20133 Milano, Italy*

Davide Faccialà − *Istituto di Fotonica e Nanotecnologie, CNR, 20133 Milano, Italy*

Caterina Vozzi − *Istituto di Fotonica e Nanotecnologie, CNR, 20133 Milano, Italy*

Lorenzo Avaldi − *CNR - Istituto di Struttura della Materia (CNR-ISM), 00133 Rome, Italy*

Paola Bolognesi − *CNR - Istituto di Struttura della Materia (CNR-ISM), 00133 Rome, Italy;* orcid.org/0000-0002-6543-6628

Mattea Carmen Castrovilli − *CNR - Istituto di Struttura della Materia (CNR-ISM), 00133 Rome, Italy;* orcid.org/0000-0002-7909-5115

Daniele Catone − *CNR - Istituto di Struttura della Materia (CNR-ISM), 00133 Rome, Italy;* orcid.org/0000-0002-7649-2756

Marcello Coreno − *CNR - Istituto di Struttura Della Materia (CNR-ISM), 34149 Trieste, Italy*

Fabio Zuccaro − *CNR - Istituto di Struttura Della Materia (CNR-ISM), 34149 Trieste, Italy*

Elisa Bernes − *Dipartimento di Scienze Chimiche, Università degli Studi di Trieste, 34127 Trieste, Italy*

Giovanna Fronzoni − *Dipartimento di Scienze Chimiche, Università degli Studi di Trieste, 34127 Trieste, Italy;* orcid.org/0000-0002-5722-2355

Daniele Toffoli − *Dipartimento di Scienze Chimiche, Università degli Studi di Trieste, 34127 Trieste, Italy;* orcid.org/0000-0002-8225-6119

Aurora Ponzi − *Institut Ruđer Bošković, 10000 Zagreb, Croatia;* orcid.org/0000-0001-9095-4366

Complete contact information is available at: https://pubs.acs.org/10.1021/acs.jpca.0c02719

Notes

The authors declare no competing financial interest.

ACKNOWLEDGMENTS

We gratefully acknowledge the assistance of our colleagues at Elettra for providing good quality synchrotron light. This research has been supported by the Croatian Science Foundation under grant no. HRZZ IP-2016-06-1142. This work has been carried out during scientific leave granted to H.S. from the University of Jordan, Amman, Jordan, during the

academic year 2018−2019. H.S. acknowledges the TRIL fellowship awarded by the Abdus Salam International Centre for Theoretical Physics (ICTP), Trieste, Italy. M.D., D.F., and C.V. acknowledge support from CNR Laboratorio Congiunto "ATTOBIO" and the Italian Ministry of Research and Education with the projects ELI and EUROFEL ESFRI Roadmap. Computational research has been supported by Finanziamento per Ricerca di Ateneo, FRA 2015 and FRA 2016, of the Università degli Studi di Trieste.

REFERENCES

(1) Sundberg, R. J. *The Chemistry of Indoles*; Academic Press: New York, 1996.
(2) Meredith, P.; Sarna, T. The Physical and Chemical Properties of Eumelanin. *Pigm. Cell Res.* **2006**, *19*, 572−594.
(3) Fuke, K.; Yoshiuchi, H.; Kaya, K. Electronic Spectra and Tautomerism of Hydrogen-Bonded Complexes of 7-Azaindole in a Supersonic Jet. *J. Phys. Chem.* **1984**, *88*, 5840−5844.
(4) Sakota, K.; Okabe, C.; Nishi, N.; Sekiya, H. Excited-State Double-Proton Transfer in the 7-Azaindole Dimer in the Gas Phase. 3. Reaction Mechanism Studied by Picosecond Time-Resolved REMPI Spectroscopy. *J. Phys. Chem. A* **2005**, *109*, 5245−5247.
(5) Fuke, K.; Ishikawa, H. Dynamics of Proton Transfer Reactions of Model Base Pairs in Theground and Excited States: Revisited. *Chem. Phys. Lett.* **2015**, *623*, 117−129.
(6) Zhang, L. S.; Davies, S. S. Microbial Metabolism of Dietary Components to Bioactive Metabolites: Opportunities for New Therapeutic Interventions. *Genome Med.* **2016**, *8*, 46.
(7) Deletioğlu, D.; Hasdemir, E.; Solak, A. O.; Üstündağ, Z.; Güzel, R. Preparation and Characterization of Poly(Indole-3-Carboxaldehyde) Film at the Glassy Carbon Surface. *Thin Solid Films* **2010**, *519*, 784−789.
(8) Ghita, M.; Arrigan, D. W. Electrochemical Overoxidation of Polyindole and Its Cation-Permselective Behavior. *Electroanalysis* **2004**, *16*, 979−987.
(9) Roman, G.; Pappas, A. C.; Kovala-Demertzi, D.; Prodromidis, M. I. Preparation of a 2-(4-Fluorophenyl)Indole-Modified Xerogel and Its Use for the Fabrication of Screen-Printed Electrodes for the Electrocatalytic Determination of Sulfide. *Anal. Chim. Acta* **2004**, *523*, 201−207.
(10) Udum, Y. A.; Düdükcü, M.; Köleli, F. Electrochemical Polymerization and Spectroscopic Investigation of 2-Methylindole. *React. Funct. Polym.* **2008**, *68*, 861−867.
(11) Talbi, H.; Monard, G.; Loos, M.; Billaud, D. Theoretical Study of Indole Polymerization. *J. Mol. Struct: THEOCHEM* **1998**, *434*, 129−134.
(12) Philips, L. A.; Levy, D. H. The Rotationally Resolved Electronic Spectrum of Indole in the Gas Phase. *J. Chem. Phys.* **1986**, *85*, 1327−1332.
(13) Berden, G.; Meerts, W. L.; Jalviste, E. Rotationally Resolved Ultraviolet Spectroscopy of Indole, Indazole, and Benzimidazole: Inertial Axis Reorientation in the $S_1(^1L_b)\leftarrow S_0$ Transitions. *J. Chem. Phys.* **1995**, *103*, 9596−9606.
(14) Brand, C.; Küpper, J.; Pratt, D. W.; Meerts, W. L.; Krügler, D.; Tatchen, J.; Schmitt, M. Vibronic Coupling in Indole: I. Theoretical Description of the $^1L_a-^1L_b$ Interaction and the Electronic Spectrum. *Phys. Chem. Chem. Phys.* **2010**, *12*, 4968−4979.
(15) Küpper, J.; Pratt, D. W.; Meerts, L.; Brand, C.; Tatchen, J.; Schmitt, M. Vibronic Coupling in Indole: II. Investigation of the $^1L_a-^1L_b$ Interaction Using Rotationally Resolved Electronic Spectroscopy. *Phys. Chem. Chem. Phys.* **2010**, *12*, 4980−4988.
(16) Korter, T. M.; Pratt, D. W.; Küpper, J. Indole−H_2O in the Gas Phase. Structures, Barriers to Internal Motion, and $S_1 \leftarrow S_0$ Transition Moment Orientation. Solvent Reorganization in the Electronically Excited State. *J. Phys. Chem. A* **1998**, *102*, 7211−7216.
(17) Kang, C.; Korter, T. M.; Pratt, D. W. Experimental Measurement of the Induced Dipole Moment of an Isolated Molecule in Its Ground and Electronically Excited States: Indole and Indole−H_2O. *J. Chem. Phys.* **2005**, *122*, 174301.
(18) Nesvadba, R.; Studecký, T.; Uhlíková, T.; Urban, Š. Microwave Spectrum and Molecular Constants of Indole. *J. Mol. Spectrosc.* **2017**, *339*, 6−11.
(19) Short, K. W.; Callis, P. R. Evidence of Pure ^1L_b Fluorescence from Redshifted Indole-Polar Solvent Complexes in a Supersonic Jet. *J. Chem. Phys.* **1998**, *108*, 10189.
(20) Montero, R.; Conde, A. P.; Ovejas, V.; Castaño, F.; Longarte, A. Ultrafast Photophysics of the Isolated Indole Molecule. *J. Phys. Chem. A* **2012**, *116*, 2698−2703.
(21) Livingstone, R.; Schalk, O.; Boguslavskiy, A. E.; Wu, G.; Bergendahl, L. T.; Stolow, A.; Paterson, M. J.; Townsend, D. Following the Excited State Relaxation Dynamics of Indole and 5-Hydroxyindole Using Time-Resolved Photoelectron Spectroscopy. *J. Chem. Phys.* **2011**, *135*, 194307.
(22) Godfrey, T. J.; Yu, H.; Biddle, M. S.; Ullrich, S. A Wavelength Dependent Investigation of the Indole Photophysics via Ionization and Fragmentation Pump−Probe Spectroscopies. *Phys. Chem. Chem. Phys.* **2015**, *17*, 25197−25209.
(23) Godfrey, T. J.; Yu, H.; Ullrich, S. Investigation of Electronically Excited Indole Relaxation Dynamics via Photoionization and Fragmentation Pump-Probe Spectroscopy. *J. Chem. Phys.* **2014**, *141*, No. 044314.
(24) Oliver, T. A. A.; Kingz, G. A.; Ashfold, M. N. R. Position Matters: Competing O−H and N−H Photodissociation Pathways in Hydroxy- and Methoxy-Substituted Indoles. *Phys. Chem. Chem. Phys.* **2011**, *13*, 14646−14662.
(25) Callis, P. R.; Vivian, J. T.; Slater, L. S. Ab Initio Calculations of Vibronic Spectra for Indole. *Chem. Phys. Lett.* **1995**, *244*, 53−58.
(26) Sundaraganesan, N.; Umamaheswari, H.; Joshua, B. D.; Meganathan, C.; Ramalingam, M. Molecular Structure and Vibrational Spectra of Indole and Ab Initio Hartree-Fock Calculations. *J. Mol. Struct., THEOCHEM* **2008**, *850*, 84−93.
(27) Catalán, J.; de Paz, J. L. G. The Molecular Geometry of Indole. *J. Mol. Struct. THEOCHEM* **1997**, *401*, 189−192.
(28) Smith, B. J.; Liu, R. A Theoretical Investigation of Indole Tautomers. *J. Mol. Struct. THEOCHEM* **1999**, *491*, 211−222.
(29) Caminati, W.; Di Bernardo, S. Microwave Spectrum and Amino Hydrogen Location in Indole. *J. Mol. Struct.* **1990**, *240*, 253−262.
(30) Reva, I.; Lapinski, L.; Lopes Jesus, A. J.; Nowak, M. J. Photoinduced Transformations of Indole and 3-Formylindole Monomers Isolated in Low-Temperature Matrices. *J. Chem. Phys.* **2017**, *147*, 194304.
(31) Nowak, M. J.; Reva, I.; Rostkowska, H.; Lapinski, L. UV-Induced Hydrogen-Atom Transfer and Hydrogen-Atom Detachment in Monomeric 7-Azaindole Isolated in Ar and n-H_2 Matrices. *Phys. Chem. Chem. Phys.* **2017**, *19*, 11447−11454.
(32) Eland, J. H. D. Photoelectron Spectra of Conjugated Hydrocarbons and Heteromolecules. *Int. J. Mass Spectrom. Ion Phys.* **1969**, *2*, 471−484.
(33) Domelsmith, L. N.; Munchausen, L. L.; Houk, K. N. Photoelectron Spectra of Psychotropic Drugs. 1. Phenethylamines, Tryptamines, and LSD. *J. Am. Chem. Soc.* **1977**, *99*, 4311−4321.
(34) Kovač, B.; Klasinc, L.; Stanovnik, B.; Tišler, M. Photoelectron Spectroscopy of Heterocycles. Azaindenes and Azaindolizines. *J. Heterocycl. Chem.* **1980**, *17*, 689−694.
(35) Fuke, K.; Yoshiuchi, H.; Kaya, K.; Achiba, Y.; Sato, K.; Kimura, K. Multiphoton Ionization Photoelectron Spectroscopy and Two-Color Multiphoton Ionization Threshold Spectroscopy on the Hydrogen Bonded Phenol and 7-Azaindole an a Supersonic Jet. *Chem. Phys. Lett.* **1984**, *108*, 179−184.
(36) Chrostowska, A.; Xu, S.; Mazière, A.; Boknevitz, K.; Li, B.; Abbey, E. R.; Dargelos, A.; Graciaa, A.; Liu, S.-Y. UV-Photoelectron Spectroscopy of BN Indoles: Experimental and Computational Electronic Structure Analysis. *J. Am. Chem. Soc.* **2014**, *136*, 11813−11820.

https://dx.doi.org/10.1021/acs.jpca.0c02719
J. Phys. Chem. A 2020, 124, 4115−4127

(37) Kierspel, T.; Bomme, C.; Di Fraia, M.; Wiese, J.; Anielski, D.; Bari, S.; Boll, R.; Erk, B. M.; Kienitz, J. S.; Müller, N. L. M.; et al. *Phys. Chem. Chem. Phys.* **2018**, *20*, 20205−20216.
(38) Plekan, O.; Feyer, V.; Richter, R.; Coreno, M.; Prince, K. C. Valence Photoionization and Photofragmentation of Aromatic Amino Acids. *Mol. Phys.* **2008**, *106*, 1143−1153.
(39) Zhang, W.; Carravetta, V.; Plekan, O.; Feyer, V.; Richter, R.; Coreno, M.; Prince, K. C. Electronic Structure of Aromatic Amino Acids Studied by Soft X-Ray Spectroscopy. *J. Chem. Phys.* **2009**, *131*, No. 035103.
(40) Maris, A.; Melandri, S.; Evangelisti, L.; Caminati, W.; Giuliano, B. M.; Plekan, O.; Feyer, V.; Richter, R.; Coreno, M.; Prince, K. C. Soft X-Ray Photoemission Spectroscopy of Selected Neurotransmitters in the Gas Phase. *J. Electron Spectrosc. Relat. Phenom.* **2012**, *185*, 244−251.
(41) Frisch, M. J.; Trucks, G. W.; Schlegel, H.B.; Scuseria, G. E.; Robb, M. A.; Cheeseman, J. R.; Scalmani, G.; Barone, V.; Petersson, G. A.; Nakatsuji, H.; et al. *Gaussian 09,* Revision A. 02; Gaussian Inc.: Wallingford, CT, 2016.
(42) Supplementary materials.
(43) von Niessen, W.; Schirmer, J.; Cederbaum, L. S. Computational Methods for the One-Particle Green's Function. *Comp. Phys. Rep.* **1984**, *1*, 57−125.
(44) Cederbaum, L. S.; Domke, W.; Schirmer, J.; von Niessen, W. Correlation Effects in the Ionization of Molecules: Breakdown of the Molecular Orbital Picture. *Adv. Chem. Phys.* **1986**, *65*, 115−159.
(45) Cederbaum, L. S.; Domke, W. Theoretical Aspects of Ionization Potentials and Photoelectron Spectroscopy: A Green's Function Approach. *Adv. Chem. Phys.* **1977**, *36*, 205−344.
(46) Ortiz, J. V. Partial Third-Order Quasiparticle Theory: Comparison for Closed-Shell Ionization Energies and an Application to the Borazine Photoelectron Spectrum. *J. Chem. Phys.* **1996**, *104*, 7599−7605.
(47) Ortiz, J. V. An Efficient, Renormalized Self-Energy for Calculating the Electron Binding Energies of Closed-Shell Molecules and Anions. *Int. J. Quantum Chem.* **2005**, *105*, 803−808.
(48) Corzo, H. H.; Galano, A.; Dolgounitcheva, O.; Zakrzewski, V. G.; Ortiz, J. V. NR2 and P3+: Accurate, Efficient Electron-Propagator Methods for Calculating Valence, Vertical Ionization Energies of Closed-Shell Molecules. *J. Phys. Chem. A* **2015**, *119*, 8813−8821.
(49) Parr, R. G.; Yang, W. *Density Functional Theory of Atoms and Molecules*; Oxford University Press: New York, 1989.
(50) Becke, A. D. Density-Functional Thermochemistry. III. The Role of Exact Exchange. *J. Chem. Phys.* **1993**, *98*, 5648−5652.
(51) Perdew, J. P. Density-Functional Approximation for The Correlation Energy of the Inhomogeneous Electron Gas. *Phys. Rev. B: Condens. Matter* **1986**, *33*, 8822−8824.
(52) Fonseca Guerra, C.; Snijders, J. G.; te Velde, G.; Baerends, E. J. Towards an Order-N DFT Method. *Theor. Chem. Acc.* **1998**, *99*, 391−403.
(53) Blyth, R. R.; Delaunay, R.; Zitnik, M.; Krempasky, J.; Krempaska, R.; Slezak, J.; Prince, K. C.; Richter, R.; Vondracek, M.; Camilloni, R.; et al. The High Resolution Gas Phase Photoemission Beamline, Elettra. *J. Electron Spectrosc. Relat. Phenom.* **1999**, *101-103*, 959−964.
(54) Derossi, A.; Lama, F.; Piacentini, M.; Prosperi, T.; Zema, N. High Flux and High Resolution Beamline for Elliptically Polarized Radiation in the Vacuum Ultraviolet and Soft X-Ray Regions. *Rev. Sci. Instrum.* **1995**, *66*, 1718−1720.
(55) Plekan, O.; Coreno, M.; Feyer, V.; Moise, A.; Richter, R.; de Simone, M.; Sankari, R.; Prince, K. C. Electronic State Resolved PEPICO Spectroscopy of Pyrimidine. *Phys. Scr.* **2008**, *78*, 058105.
(56) *Baspik 43x63 mm*. https://baspik.com/eng/products/mkp/dec43_63//
(57) Torelli, P.; Sacchi, M.; Cautero, G.; Cautero, M.; Krastanov, B.; Lacovig, P.; Pittana, P.; Sergo, R.; Tommasini, R.; Fondacaro.; et al. Experimental Setup for High Energy Photoemission Using Synchrotron Radiation. *Rev. Sci. Instrum.* **2005**, *76*, No. 023909.
(58) Cautero, G.; Sergo, R.; Stebel, L.; Lacovig, P.; Pittana, P.; Predonzani, M.; Carrato, S. A Two-Dimensional Detector for Pump-and-Probe and Time Resolved Experiments. *Nucl. Instrum. Methods Phys. Res. A* **2008**, *595*, 447−459.
(59) Sa'adeh, H. et al., *Valence PEPICO of Indole and Its Derivatives in the Gas Phase*. (in preparation).
(60) Kimura, K.; Katsumata, S.; Achiba, Y.; Yamazaki, T.; Iwata, S. *Handbook of HeI Photoelectron Spectra of Fundamental Organic Molecules;* Japan Scientific Societies: Tokyo, 1981.
(61) Myrseth, V.; Bozek, J. D.; Kukk, E.; Sæthre, L. J.; Thomas, T. D. Adiabatic and Vertical Carbon 1s Ionization Energies in Representative Small Molecules. *J. Electron Spectrosc. Relat. Phenom.* **2002**, *122*, 57−63.
(62) Petterson, L.; Nordegren, J.; Selander, L.; Nordling, C.; Siegbahn, K.; Ågren, H. Core-Electron Binding Energies in the Soft X-Ray Range Obtained in X-Ray Emission. *J. Electron Spectrosc. Relat. Phenom.* **1982**, *27*, 29−37.
(63) Thomas, T. D.; Shaw, R. W., Jr. Accurate Core Ionization Potentials and Photoelectron Kinetic Energies for Light Elements. *J. Electron Spectrosc. Relat. Phenom.* **1974**, *5*, 1081−1094.
(64) Gelius, U.; Allan, C. J.; Johansson, G.; Siegbahn, H.; Allison, D. A.; Siegbahn, K. The ESCA Spectra of Benzene and the Iso-Electronic Series, Thiophene, Pyrrole and Furan. *Phys. Scr.* **1971**, *3*, 237−242.
(65) Lemmon, E. W.; McLinden, M. O.; Friend, D. G.; Linstrom, P.; Mallard, W. *NIST Chemistry WebBook, NIST Standard Reference Database Number 69*; National Institute of Standards and Technology: Gaithersburg, MD, http://webbook.nist.gov/
(66) Calais, J.-L.; Kryachko, E. *Conceptual Perspectives in Quantum Chemistry;* Springer, 1997.
(67) Ferreira, A. M., Seabra, G., Dolgounitcheva, O., Zakrzewski, V. G., Ortiz, J. V. Application and Testing of Diagonal, Partial Third-Order Electron Propagator Approximations. In: Cioslowski, J.; Eds.; *Quantum-Mechanical Prediction of Thermochemical Data*; Understanding Chemical Reactivity: Springer, Dordrecht, 2001, pp 131−160.
(68) Snis, A.; Matar, S. F.; Plashkevych, O.; Ågren, H. Core Ionization Energies of Carbon−Nitrogen Molecules and Solids. *J. Chem. Phys.* **1999**, *111*, 9678−9686.
(69) Chong, D. P. Computational Study of the Structures and Photoelectron Spectra of 12 Azabenzenes. *Can. J. Chem.* **2019**, *97*, 697−703.
(70) Sankari, R.; Ehara, M.; Nakatsuji, H.; Senba, Y.; Hosokawa, K.; Yoshida, H.; De Fanis, A.; Tamenori, Y.; Aksela, S.; Ueda, K. Vibrationally Resolved O 1s Photoelectron Spectrum of Water. *Chem. Phys. Lett.* **2003**, *380*, 647−653.
(71) Barber, M.; Bell, D. J.; Morris, M.; Tetler, L. W.; Woods, M. D.; Monaghan, J. J.; Morden, W. E. Mass Spectra of Doubly Charged Ions. *Org. Mass Spectrom.* **1989**, *24*, 504−510.
(72) Eland, J. H. D.; Feifel, R. *Double Photoionisation Spectra of Molecules. Oxford University Press*, 2018.
(73) Perreault, H.; Ramaley, L.; Benoit, F. M.; Sim, P. G.; Boyd, R. K. Fragmentation Reactions of Molecular Dications of Aromatic Heterocyclic Fused-Ring Compounds Containing More than One Nitrogen Atom. *Org. Mass Spectrom.* **1992**, *27*, 89−96.
(74) Carlson, T. A. *Photoelectron and Auger Spectroscopy*; Plenum Press: New York, 1975.
(75) Püttner, R.; Sekushin, V.; Kaindl, G.; Liu, X.-J.; Fukuzawa, H.; Ueda, K.; Tanaka, T.; Hoshino, M.; Tanaka, H. A Vibrationally Resolved C $1s^{-1}$ Auger Spectrum of CO_2. *J. Phys. B: At., Mol. Opt. Phys.* **2008**, *41*, 045103.
(76) Siegbahn, K.; Nordling, C.; Johansson, G.; Hedman, J.; Heden, P. F.; Hamrin, K.; Gelius, U.; Bergmark, T.; Werme, L. O.; Manne, R.; et al. *ESCA Applied to Free Molecules;* North-Holland Publ. Co.: Amsterdam-London, 1971.
(77) Werner, H.-J.; Knowles, P. J. An Efficient Internally Contracted Multiconfiguration−Reference Configuration Interaction Method. *J. Chem. Phys.* **1988**, *89*, 5803−5814.

https://dx.doi.org/10.1021/acs.jpca.0c02719
J. Phys. Chem. A 2020, 124, 4115−4127

(78) Werner, H.-J.; Knowles, P. J.; Knizia, G.; Manby, F. R.; Schütz, M. Molpro: A General-Purposequantum Chemistry Program Package. *Software Focus* **2012**, *2*, 242−253.
(79) Storchi, L.; Tarantelli, F.; Veronesi, S.; Bolognesi, P.; Fainelli, E.; Avaldi, L. The Auger Spectroscopy of Pyrimidine and Halogen-Substituted Pyrimidines. *J. Chem. Phys.* **2008**, *129*, 154309.
(80) Eland, J. H. D. Spectra of the Dications of Benzene, Naphthalene and Azulene. *Chem. Phys.* **2008**, *345*, 82−86.
(81) Molloy, R. D.; Danielsson, A.; Karlsson, L.; Eland, J. H. D. Double Photoionisation Spectra of Small Molecules and a New Empirical Rule for Double Ionisation Energies. *Chem. Phys.* **2007**, *335*, 49−54.

https://dx.doi.org/10.1021/acs.jpca.0c02719
J. Phys. Chem. A 2020, 124, 4115−4127